

# Characterisation and Activity of Praseodymium Oxide Catalysts prepared in Different Gases from Praseodymium Oxalate Hydrate

## Microscopic, Thermogravimetric and IR Spectroscopic Studies

Gamal A. M. Hussein

Chemistry Department Faculty of Science, Minia University, El-Minia 61519, Egypt

$\text{PrO}_{1.833}$  and  $\text{Pr}_2\text{O}_3$  catalysts have been obtained as final decomposition products of  $\text{Pr}_2(\text{C}_2\text{O}_4)_3 \cdot 10\text{H}_2\text{O}$  in different gases ( $\text{O}_2$ ,  $\text{N}_2$  and  $\text{H}_2$ ). The decomposition processes were characterized by thermogravimetric (TG) and differential thermal analysis (DTA), X-ray diffraction (XRD) and IR spectroscopy of the solid-phase products. The results indicate that the compound dehydrates in three steps at 100, 150 and 380 °C and that the anhydrous oxalate decomposes at 445 °C to form two phases of  $\text{Pr}_2\text{O}_2(\text{CO}_3)$  depending upon the atmosphere used for the reaction. On further heating  $\text{PrO}_{1.833}$  is formed at 550 °C in  $\text{O}_2$  and at 650 °C in  $\text{N}_2$ . In contrast,  $\text{Pr}_2\text{O}_3$  was formed at 650 °C in  $\text{H}_2$ . Surface area measurements and scanning electron microscopy (SEM) have shown that  $\text{PrO}_{1.833}$  produced at 700 °C has a different surface area depending on the gas used: 43 and 64  $\text{m}^2 \text{g}^{-1}$  for  $\text{O}_2$  and  $\text{N}_2$ , respectively. The surface area of  $\text{Pr}_2\text{O}_3$  formed in  $\text{H}_2$  is 59  $\text{m}^2 \text{g}^{-1}$ . The texture of the catalyst has been found to depend upon the decomposition atmosphere.

IR spectroscopy has been used to analyse (qualitatively and quantitatively) the gas-phase reaction products between room temperature and 400 °C from the dehydrogenation and dehydration reactions of propan-2-ol over  $\text{PrO}_{1.833}$  and  $\text{Pr}_2\text{O}_3$  catalysts. The results revealed that  $\text{Pr}_2\text{O}_3$  is a selective dehydration catalyst at 275 °C, decomposing propan-2-ol into propene (ca. 80%). However,  $\text{PrO}_{1.833}$  is a dual function dehydration/dehydrogenation catalyst.

Praseodymium oxides comprise  $\text{Pr}_2\text{O}_3$ ,  $\text{PrO}_2$  and a range of intermediate phases:  $\text{PrO}_{1.833}$ ,  $\text{PrO}_{1.810}$ ,  $\text{PrO}_{1.800}$ ,  $\text{PrO}_{1.780}$ ,  $\text{PrO}_{1.714}$  and  $\text{PrO}_{1.67}$ .<sup>1–3</sup>  $\text{Pr}_2\text{O}_3$  possesses hexagonal structure,  $\text{PrO}_2$  the fluorite structure and  $\text{PrO}_{1.180}$  and  $\text{PrO}_{1.833}$  are oxygen-deficient modifications of the fluorite structure. The production of these phases depends on the precursor used and the atmosphere and temperature of decomposition.<sup>4</sup>

Moosath *et al.*<sup>5</sup> studied the decomposition of  $\text{Pr}_2(\text{C}_2\text{O}_4)_3 \cdot 4\text{H}_2\text{O}$  in air and reported that complete dehydration occurs at 370 °C, followed by rapid decomposition of anhydrous oxalate to  $\text{Pr}_2\text{O}_2\text{CO}_3$  at 480 °C. The latter decomposes at 560 °C to yield  $\text{Pr}_2\text{O}_3$  as a final product. Muraishi *et al.*<sup>6</sup> studied the decomposition of Pr malonates in an  $\text{N}_2$  atmosphere. They stated that  $\text{Pr}_2\text{O}_2\text{CO}_3$  forms as an intermediate at 329 °C and that  $\text{Pr}_2\text{O}_3$  is obtained as the final product at 617 °C.

In contrast, Dassuncao *et al.*<sup>7</sup> studied the decomposition of hydrated praseodymium basic carbonate [ $\text{Pr}_2(\text{OH})_2(\text{CO}_3)_2 \cdot \text{H}_2\text{O}$ ] in air, and stated that  $\text{Pr}_2\text{O}_2\text{CO}_3$  was formed at 460 °C and decomposed to  $\text{PrO}_{1.833}$  at 570 °C via a  $\text{Pr}_2\text{O}_{2.6}(\text{CO}_3)_{0.4}$  intermediate. In a later study,<sup>8</sup> for the decomposition of  $\text{Pr}_2(\text{C}_2\text{O}_4)_3 \cdot 10\text{H}_2\text{O}$  and  $\text{Pr}(\text{CH}_3\text{COO})_3 \cdot \text{H}_2\text{O}$  in air, it was found that both oxalate and acetate of praseodymium formed  $\text{Pr}_2\text{O}_2\text{CO}_3$  as an intermediate, which decomposes at 575 °C to give  $\text{PrO}_{1.833}$  as a final product. The main difference between the final products obtained from acetate and oxalate at 800 °C for 1 h in air is in the surface area;  $\text{PrO}_{1.833}$  obtained from Pr acetate had a surface area of 18  $\text{m}^2 \text{g}^{-1}$  and Pr oxalate 8  $\text{m}^2 \text{g}^{-1}$ .

Metal-oxide catalysts with high surface area and reactivity are often obtained from the thermal decomposition of precursor compounds.<sup>9,10</sup> The release of volatile components forces generation of fast-transport pathways (pores) through the bulk material.<sup>11,12</sup> It has been established that the surface texture and the performance of solid catalysts are critically controlled by their preparation and pretreatment conditions.<sup>12–15</sup> The decomposition of propan-2-ol has been widely used to examine the acid–base properties of metal-

oxide catalysts.<sup>16–18</sup> It is generally assumed that acidic oxides catalyse dehydration and basic oxides catalyse dehydrogenation.

In the present study the effect of the reaction atmosphere on the thermal decomposition course and final decomposition products of Pr oxalate decahydrate was examined by TG and DTA. The solid products at intermediate temperatures were subjected to IR and XRD. The final decomposition products, 700 °C for 1 h in  $\text{O}_2$ ,  $\text{H}_2$  and  $\text{N}_2$ , were subjected to surface area measurements and SEM and tested qualitatively and quantitatively for the decomposition of propan-2-ol.

### Experimental

Praseodymium oxalate decahydrate ( $\text{PrOx}$ ),  $\text{Pr}_2(\text{C}_2\text{O}_4)_3 \cdot 10\text{H}_2\text{O}$ , (Aldrich, 99.99%), was calcined at 200, 450 and 700 °C for 1 h in different atmospheres:  $\text{O}_2$ ,  $\text{H}_2$  and  $\text{N}_2$ . The calcination temperatures were chosen on the basis of the thermal analysis results (see below). Propan-2-ol and acetone (BDH, spectroscopic grade) were thoroughly degassed by freeze–pump–thaw cycles under vacuum prior to use.

### Thermal Analysis

TG and DTA of the parent material ( $\text{PrOx}$ ) were carried out using heating rates of 2–20 °C  $\text{min}^{-1}$ , up to 800 °C, in a dynamic atmosphere of  $\text{O}_2$ ,  $\text{H}_2$  or  $\text{N}_2$  (20  $\text{ml min}^{-1}$ ), using a model 30H Shimadzu analyser. 10–15 mg of the test sample were used for the TG measurements and highly sintered  $\alpha$ - $\text{Al}_2\text{O}_3$  was the thermally inert reference material for the DTA.

### IR Spectroscopy

IR spectra were obtained at a resolution of 5.3  $\text{cm}^{-1}$ , over the range 4000–400  $\text{cm}^{-1}$ , using a model 580B Perkin-Elmer spectrophotometer, equipped with a 3700 PE data station for spectral acquisition and handling.

(I) IR spectra of PrOx and its solid calcination products were obtained from thin ( $>20 \text{ mg m}^{-2}$ ), lightly loaded ( $<1\%$ ) KBr-supported discs.

(II) IR spectra of propan-2-ol and its gaseous catalytic-decomposition products were taken with the help of a specially designed variable-temperature IR cell<sup>19</sup> equipped with KBr windows. The following standard procedure was adopted. The catalyst (100 mg in powder form) was heated in a stream of oxygen at  $600^\circ\text{C}$  for 30 min to clean the surface of carbonate contamination<sup>13</sup> and cooled to room temperature under vacuum ( $10^{-3}$  Torr). Propan-2-ol (10 Torr) was allowed into the cell at various temperatures from 100 to  $400^\circ\text{C}$ , and maintained in contact with the catalyst for 10 min.

Propan-2-ol and its gaseous decomposition products were quantitatively analysed using the standard QUANT software from Perkin-Elmer and the on-line data acquisition system. Accordingly, the amounts of the gaseous components (reactant and products) were determined from calibration curves relating the IR-absorption intensity at a certain frequency to the calibrated gas pressure (Torr). The calibration curves were derived from IR data obtained from authentic samples of each of the gas-phase components under identical spectroscopic conditions. The absorption intensity was measured at  $3665 \pm 5 \text{ cm}^{-1}$  for propan-2-ol,  $1740 \pm 5 \text{ cm}^{-1}$  for acetone (the dehydrogenation product) and at  $910 \pm 5 \text{ cm}^{-1}$  for propene (the dehydration product).<sup>16</sup>

### XRD

XRD analyses of PrOx and its calcination products were carried out by means of a model JSX-60 PA Jeol diffractometer using Ni filtered Cu-K $\alpha$  radiation. For identification purposes the diffraction patterns ( $I/I^0$  vs.  $d$ -spacing) obtained were matched with ASTM standards.

### N<sub>2</sub>-adsorption Measurements

N<sub>2</sub>-sorption isotherms were determined volumetrically at  $-196^\circ\text{C}$  using microapparatus based on a design described by Lippens *et al.*<sup>20</sup> The test samples were outgassed at  $200^\circ\text{C}$  for 2 h while evacuating at  $10^{-5}$  Torr.

### Electron Microscopy

Samples of the final decomposition product ( $700^\circ\text{C}$ ) were examined in a Jeol 35CF scanning electron microscope to characterize the texture. Before examination, the samples were rendered conducting by pre-coating with a thin film of Au-Pd.

## Results and Discussion

TG and DTA curves for PrOX heated up to  $800^\circ\text{C}$  at a rate of  $10^\circ\text{C min}^{-1}$  in O<sub>2</sub>, H<sub>2</sub> and N<sub>2</sub> atmospheres are shown in Fig. 1. IR spectra and XRD powder patterns obtained for PrOx and its solid decomposition products at 250, 450 and  $700^\circ\text{C}$  are shown in Fig. 2 and 3. Fig. 4A shows the N<sub>2</sub>-sorption isotherms for PrOx calcined at  $700^\circ\text{C}$  for 1 h in different gases. The corresponding pore-volume-distribution curves are given in Fig. 4B. The SEM for the same samples are shown in Fig. 5. Fig. 6A shows the IR gas-phase spectra from 10 Torr of propan-2-ol in contact with PrOx ( $700^\circ\text{C}$  in O<sub>2</sub>) after consecutive 10 min periods at the temperatures indicated. Quantitative analysis of the gas-phase composition, resulting from 10 Torr of propan-2-ol giving rise to acetone and propene, after consecutive 10 min intervals at the temperatures indicated over the PrOx ( $700^\circ\text{C}$  in O<sub>2</sub> and H<sub>2</sub>) catalysts, is given in Fig. 6B.

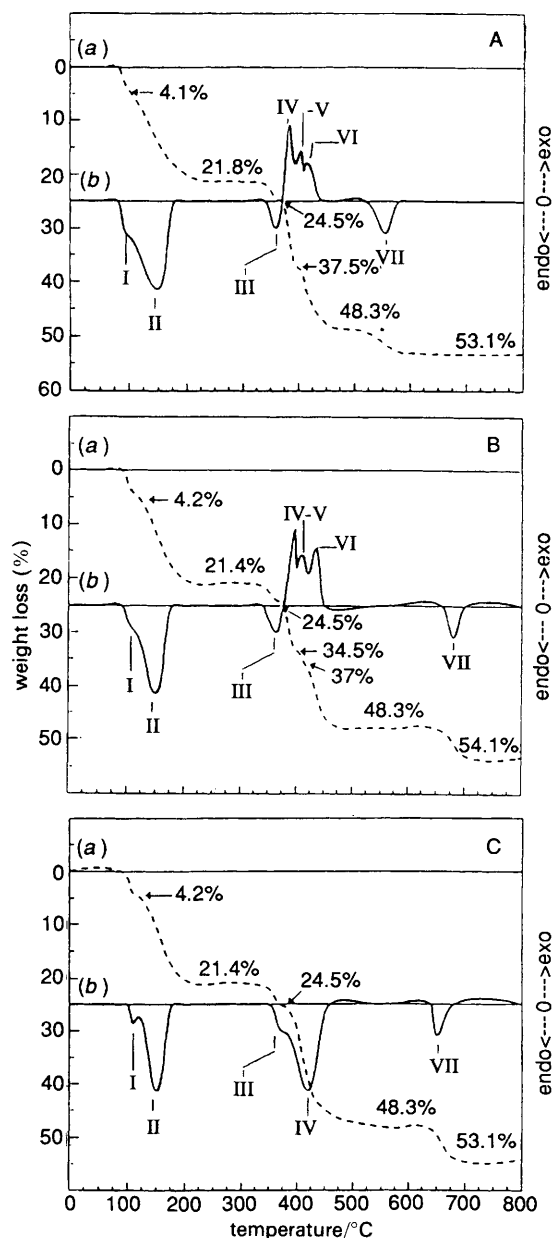
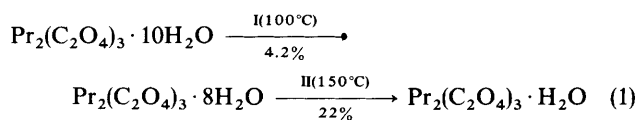


Fig. 1 TG (a) and DTA (b) curves for PrOx measured in a dynamic atmosphere ( $20 \text{ ml min}^{-1}$ ) of A, O<sub>2</sub>; B, N<sub>2</sub> and C, H<sub>2</sub>; at a heating rate of  $10^\circ\text{C min}^{-1}$ . DTA peak labels I–VII are discussed in the text and occur at temperatures ( $^\circ\text{C}$  for I–VII); A: 100, 150, 375, 390, 415, 425, 550; B: 110, 150, 370, 390, 415, 445, 675; C: 110, 150, 380, 420, (no V or VI), 650.

### Characterization of the Thermal Events

#### Dehydration Processes

*Events I and II* ( $100$ – $150^\circ\text{C}$ ). The TG and DTA curves (Fig. 1) show that processes I and II are overlapping endothermic weight-loss (WL) processes. The WL observed (21.8%) from both processes is very close to that expected for release of 9 mol of water (22.3%).



As reported earlier,<sup>8</sup> the IR spectrum of the solid phase at  $200^\circ\text{C}$  (Fig. 2) bears a great deal of similarity to that for unheated PrOx because both show absorption bands arising

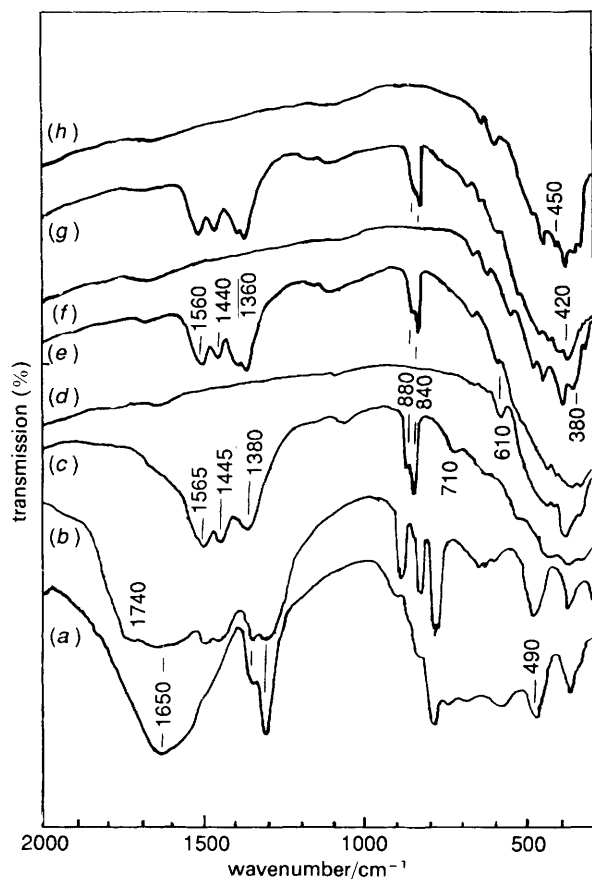


Fig. 2 IR spectra of (a) KBr-supported PrOX and its solid decomposition products taken at room temperature after heating for 1 h in (b) O<sub>2</sub>-H<sub>2</sub>-N<sub>2</sub> at 200 °C, (c) O<sub>2</sub> at 450 °C, (d) O<sub>2</sub> at 700 °C, (e) H<sub>2</sub> at 450 °C, (f) H<sub>2</sub> at 700 °C, (g) N<sub>2</sub> at 450 °C and (h) N<sub>2</sub> at 700 °C

from oxalate. However, the corresponding XRD pattern (Fig. 3) indicates that the products are amorphous and so water of hydration is very important for the coherency of the PrOX crystal.<sup>10</sup>

**Event III (375 °C).** Process III largely overlaps with process IV and brings the total WL to 24.5%, close to that expected (24.8%) for the complete dehydration of PrOX. These results

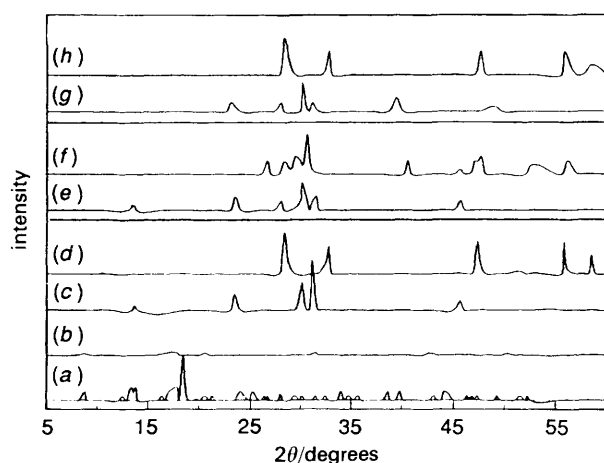


Fig. 3 XRD powder patterns of (a) PrOX and its decomposition products taken at room temperature after heating for 1 h in (b) O<sub>2</sub>-H<sub>2</sub>-N<sub>2</sub> at 200 °C, (c) O<sub>2</sub> at 450 °C to give Pr<sub>2</sub>O<sub>2</sub>CO<sub>3</sub> (II), (d) O<sub>2</sub> at 700 °C to give Pr<sub>0.1833</sub>, (e) H<sub>2</sub> at 450 °C to give Pr<sub>2</sub>O<sub>2</sub>CO<sub>3</sub> (I), (f) H<sub>2</sub> at 700 °C to give Pr<sub>2</sub>O<sub>3</sub>, (g) N<sub>2</sub> at 450 °C to give Pr<sub>2</sub>O<sub>2</sub>CO<sub>3</sub> (I) and (h) N<sub>2</sub> at 700 °C to give Pr<sub>0.1833</sub>

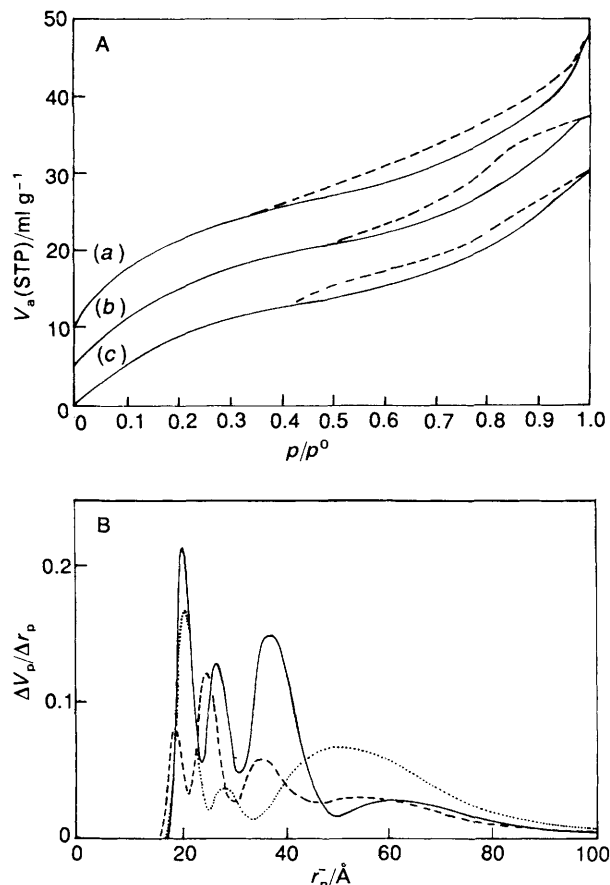
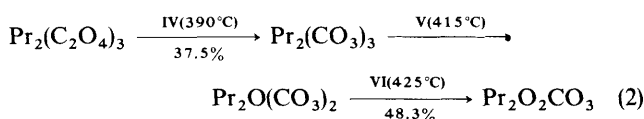


Fig. 4 A, BET N<sub>2</sub>-sorption isotherm at -196 °C for PrOX calcined for 1 h at 700 °C in (a) N<sub>2</sub>, (b) O<sub>2</sub> and (c) H<sub>2</sub>. B, Pore-volume distribution curves for the same system: (—) N<sub>2</sub>, (---) O<sub>2</sub> and (····) H<sub>2</sub>.

are in agreement with the earlier study,<sup>8</sup> for the dehydration of PrOX in air, *i.e.* the dehydration of PrOX is not affected by the gaseous atmosphere.

#### Decomposition Processes in Oxygen

**Events IV, V and VI (390–425 °C).** Fig. 1A shows that processes IV, V and VI are overlapping exothermic WL processes. The TG curve shows that these processes are responsible for the decomposition of anhydrous PrOX to Pr<sub>2</sub>O<sub>2</sub>CO<sub>3</sub>, as indicated by the observed WL (48.3%) which is very close to that expected (48.6%) for the formation of Pr<sub>2</sub>O<sub>2</sub>CO<sub>3</sub> from unstable Pr<sub>2</sub>(C<sub>2</sub>O<sub>4</sub>)<sub>3</sub> as follows<sup>8</sup>



The IR spectrum [Fig. 2(a)] and XRD pattern [Fig. 3(a)] support reaction (2). The IR spectrum displays absorptions at 1560, 1440, 880 and 840 cm<sup>-1</sup> assignable to oxycarbonate species.<sup>21</sup> The strong absorptions emerging at 650–450 cm<sup>-1</sup> are related to Pr–O vibration modes.<sup>21</sup> XRD also indicates the presence of crystalline Pr<sub>2</sub>O<sub>2</sub>CO<sub>3</sub> (II) (ASTM No. 25-696).

**Event VII (550 °C).** On further heating, process VII takes place endothermally (Fig. 1A) at 550 °C. The maximum WL thus determined (53.1%) agrees well with the theoretical value (53.09%) expected for a complete conversion of PrOX into PrO<sub>1.833</sub>, *i.e.* process VII is an oxidative decomposition process (Pr<sup>3+</sup> → Pr<sup>3.66+</sup>).

The IR spectrum of PrOX treated at 700 °C (Fig. 2) declares the absence of detectable absorptions arising from oxycarb-

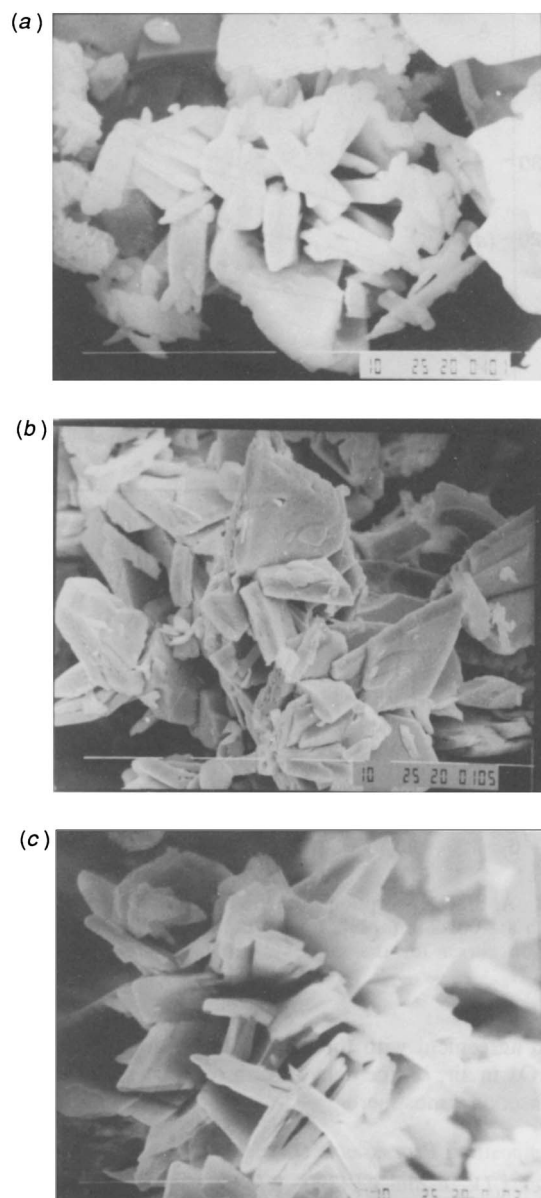


**Fig. 5** SEM micrographs (2500 $\times$ ) for PrOx calcined for 1 h at 700 °C in (a) N<sub>2</sub>, (b) H<sub>2</sub> and (c) O<sub>2</sub>

onate species. However, the absorptions below 850 cm<sup>-1</sup>, which are related to lattice-vibration modes of Pr—O, are retained.<sup>21</sup> The corresponding XRD for PrOx at 700 °C (Fig. 3) shows only the pattern for crystalline PrO<sub>1.833</sub> (ASTM No. 6-329).

In comparison with the earlier study in air,<sup>8</sup> it is clear that the decomposition of PrOx in O<sub>2</sub> is nearly identical to that obtained in air.

#### Decomposition Processes in Hydrogen

Fig. 1B shows that the decomposition of PrOx in hydrogen is nearly similar to that obtained in oxygen (Fig. 1A), especially considering the number and nature of the thermal events involved. The main differences are (i) reaction (2) in processes IV, V and VI probably takes place as

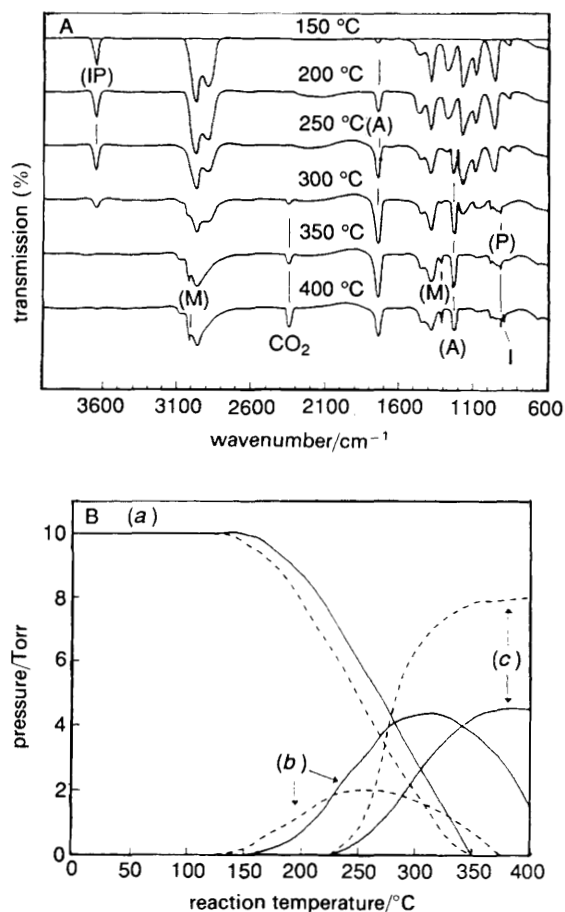
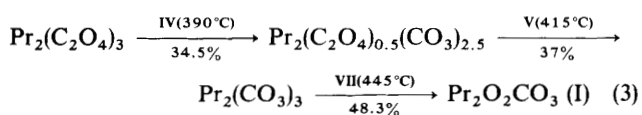


**Fig. 6** A, IR spectra of (IP) propan-2-ol (10 Torr) and its decomposition products [(A) acetone, (P) propene, (M) methane, (I) isobutene] in contact with PrO<sub>1.833</sub> for 10 min at the indicated temperatures. B, IR quantitative analysis of the gas-phase composition resulting from 10 Torr of (a) propan-2-ol decomposing over (—) PrO<sub>1.833</sub> and (---) Pr<sub>2</sub>O<sub>3</sub> to give (b) acetone and (c) propene. Measurements made after consecutive 10 min intervals at the temperatures indicated in A.

The WL observed throughout process IV is 34.5% which is very close to that calculated (34.4%) for the formation of Pr<sub>2</sub>(C<sub>2</sub>O<sub>4</sub>)<sub>0.5</sub>(CO<sub>3</sub>)<sub>2.5</sub> and so the H<sub>2</sub> atmosphere retards the formation of both Pr<sub>2</sub>(CO<sub>3</sub>)<sub>3</sub> and Pr<sub>2</sub>O<sub>2</sub>CO<sub>3</sub>. (ii) The structure of Pr<sub>2</sub>O<sub>2</sub>CO<sub>3</sub> (I) (ASTM No. 37-805) formed in H<sub>2</sub> is different from that obtained in O<sub>2</sub> at 450 °C [Fig. 3(e)]. (iii) Process VII is shifted to higher temperature (675 °C, Fig. 1B), also the WL observed is 54.1%, close to that calculated (54.5%) for the formation of Pr<sub>2</sub>O<sub>3</sub>. XRD at 700 °C [Fig. 3(b)] reveals the formation of the hexagonal structure Pr<sub>2</sub>O<sub>3</sub> (ASTM No. 6-410) and so the oxidation state of Pr does not change during the decomposition in hydrogen.

#### Decomposition Processes in Nitrogen

The decomposition of anhydrous PrOx in nitrogen (Fig. 1C) takes place through one large endothermic effect located at 420 °C. The WL observed by the end of process IV is 48.3%, which is very close to that (48.6%) calculated for the formation of Pr<sub>2</sub>O<sub>2</sub>CO<sub>3</sub>. The XRD, Fig. 3(g), reveals the formation of Pr<sub>2</sub>O<sub>2</sub>CO<sub>3</sub> (I) and so in both N<sub>2</sub> and H<sub>2</sub> the Pr<sub>2</sub>O<sub>2</sub>CO<sub>3</sub> formed had the same structure. However, the Pr<sub>2</sub>O<sub>2</sub>CO<sub>3</sub> thus formed in an N<sub>2</sub> atmosphere decomposed at 650 °C (Fig. 1C) to give PrO<sub>1.833</sub> as the final product, as indicated by the WL observed (53.1%) by the end of the decomposition course and by the XRD pattern of PrOx (N<sub>2</sub>) [Fig. 3(b)]. The final

decomposition step is, therefore, oxidative as in the case of  $O_2$  ( $Pr^{3+} \rightarrow Pr^{3.66+}$ ).

### Surface Characterization

All the isotherms shown in Fig. 4A are close to BET-type IV,<sup>22</sup> revealing a porous character. The hysteresis loops exhibited in Fig. 4A have almost the shape of type (B) H3. These general features indicate that the majority of the pores are slit-shaped and/or non-parallel plates.<sup>23</sup> The presence of micropores and mesopores was indicated by the pore-size distribution (PSD) curves (Fig. 4B) and texture data (Table 1). The PSD curve of PrOx (700 °C in  $O_2$ ) ( $S_{BET} = 43 \text{ m}^2 \text{ g}^{-1}$ ) exhibits mainly micropores and mesopores (three peaks at 19, 26 and 35 Å) which are probably the reason for the low surface area in comparison with the other samples. However, it has a higher area than that obtained ( $8 \text{ m}^2 \text{ g}^{-1}$ ) at 800 °C in air. The PSD curve of PrOx (700 °C in  $N_2$ ), which has the same crystal structure and composition ( $PrO_{1.833}$ ) ( $S_{BET} = 64 \text{ m}^2 \text{ g}^{-1}$ ) (three peaks at 20, 28 and 40 Å), shows growth of the mesopores which is probably responsible for the higher area in comparison to the  $O_2$  sample. On the other hand, the PSD curve and texture data of the hexagonal  $Pr_2O_3$  obtained in an  $H_2$  atmosphere ( $S_{BET} = 59 \text{ m}^2 \text{ g}^{-1}$ ) which is different in composition and structure, exhibits a wider spectrum of mesoporosity (three peaks at 22, 30 and 45–60 Å) and so the  $H_2$  affected not only the composition and structure of the final product but also the surface area and texture. The similarity of the texture data for PrOx calcined in both  $O_2$  and  $N_2$  at 700 °C is most probably because they are formed from the same  $Pr_2O_2CO_3$  (I) intermediate.

The SEM of PrOx (Fig. 5) supports the above results and reveals the presence of well formed crystals of a wide range of sizes with rough surface steps and non-parallel plate-shaped crystals. The pores are randomly distributed over the surface which was noted to be rough with extensive porosity and interplating.

### Catalytic Activity for Propan-2-ol Decomposition

IR spectra from the gas phase of propan-2-ol/ $PrO_{1.833}$  (PrOx, 700 °C in  $O_2$ ) at different temperatures are shown in Fig. 6A. The room temperature and 150 °C spectra display the characteristic bands of propan-2-ol.<sup>2</sup> At 200 °C a tiny but important absorption emerges at  $1740 \text{ cm}^{-1}$ , which developed markedly in the 250 °C spectrum together with another absorption at  $1250 \text{ cm}^{-1}$ . The two bands mark the formation of gas-phase acetone,<sup>2</sup> indicating that the dehydrogenation of propan-2-ol started at 200 °C. At 250 °C (Fig. 6A) additional absorptions emerge at 1650 (doublet) and  $915 \text{ cm}^{-1}$  that are due to propene. Hence, the dehydration of propan-2-ol occurs at 250 °C. Following the reaction at 300 °C the acetone bands are slightly intensified, the propene absorptions grow stronger and absorptions in the  $\nu_{CH}$  region ( $3100\text{--}2800 \text{ cm}^{-1}$ ) are re-structured.

**Table 1** Surface-textural characteristics of PrOx calcined at 700 °C in  $O_2$ ,  $N_2$  and  $H_2$

atmosphere	$S_{BET}$ / $\text{m}^2 \text{ g}^{-1}$	C	$V_p$ / $\text{ml g}^{-1}$	$r_{max}$ /Å
$O_2$	43	72	0.059	20, 22, 40
$N_2$	64	44	0.070	20, 27, 50
$H_2$	59	60	0.55	20, 28, 50–60

BET surface area ( $S_{BET}$ ), constant (C), pore volume ( $V_p$ ) and maximum pore radius ( $r_{max}$ ).

At 350 °C, absorptions due to alcohol are hardly detectable and acetone absorptions, while weakened, remain up to 400 °C. In contrast, absorptions due to propene are intensified. Moreover, at 350 °C new absorptions emerge at  $3010$  and  $1310 \text{ cm}^{-1}$  (due to methane),<sup>16</sup> at  $890 \text{ cm}^{-1}$  (due to isobutene) and at  $2340$  and  $670 \text{ cm}^{-1}$  (due to  $CO_2$ ).<sup>16</sup> These new absorptions are greater in the 400 °C spectrum (Fig. 6A). The formation of the  $CH_4$ , isobutene and  $CO_2$  by-products is due to surface reactions of acetone *via* an aldol-type condensation. Such reactions involve adsorbed and gas-phase acetone molecules, as well as nucleophilic surface OH groups.<sup>16,24–26</sup>

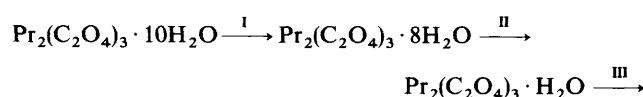
The IR gas-phase spectrum of propan-2-ol over  $Pr_2O_3$  is nearly similar to that obtained for  $PrO_{1.833}$ . The main differences observed with  $Pr_2O_3$  are (i) acetone first appeared at 200 °C and its peak grew stronger at 250 °C, but disappeared completely at 400 °C, (ii) propene first appeared at 200 °C, (iii) both  $CO_2$  and  $CH_4$  were also detected, while isobutene was not.

The above results are presented on a quantitative basis in Fig. 6B. It is clear that propan-2-ol over  $Pr_2O_3$  starts to decompose at 200 °C, acetone emerges simultaneously at 200 °C and then propene at 250 °C. The rate of alcohol decomposition appears to reach a maximum at 300 °C, as does the production of propene (*ca.* 80%) at 350 °C, and that of acetone (*ca.* 20%) at 300 °C. At 400 °C, the acetone decomposes completely. For propan-2-ol over  $PrO_{1.833}$ , the production of propene is *ca.* 50% at 325 °C. At 400 °C the amount of acetone commences to decrease.

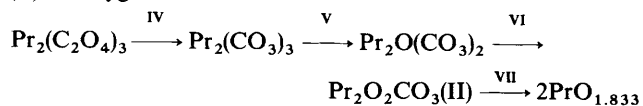
These activity and selectivity results for both  $Pr_2O_3$  and  $PrO_{1.833}$  in the decomposition of propan-2-ol may indicate that  $Pr_2O_3$  (hexagonal structure) is more acidic (highly active dehydration catalyst)<sup>27</sup> than  $PrO_{1.833}$ . The high dehydrogenation activity of  $PrO_{1.833}$  also reveals the basicity. However, acetone formation can occur by a redox mechanism.<sup>27</sup>

### Conclusion

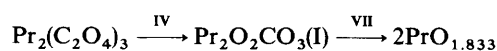
(1) The thermal decomposition of PrOx in different atmospheres involves the following pathways:



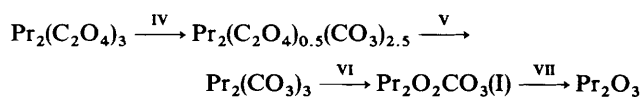
(A) In oxygen



(B) In nitrogen



(C) In hydrogen



(2) The dehydration processes are not affected by the nature of the atmosphere. The water of hydration is responsible for the crystal coherency of PrOx. (3) Two different phases of  $Pr_2O_2CO_3$  were detected as stable intermediates during the decomposition of PrOx. These depend upon the atmosphere. (4) PrOx decomposes to  $PrO_{1.833}$  in  $O_2$  and  $N_2$ . However, the hexagonal  $Pr_2O_3$  was formed as a final product in  $H_2$ . (5) The decomposition processes and the final decomposition products are mainly controlled by the nature of the atmosphere. (6) Pr oxides obtained at 700 °C have surface areas of

32 (in O<sub>2</sub>), 64 (in N<sub>2</sub>) and 59 m<sup>2</sup> g<sup>-1</sup> (in H<sub>2</sub>) and have two different types of porosity (micropores and mesopores). (7) Pr<sub>2</sub>O<sub>3</sub> obtained at 700 °C is a selective catalyst for the dehydration of propan-2-ol (to form propene, ca. 80%, maximized at 300 °C), with a lesser tendency for dehydrogenation (to form acetone, ca. 10% maximized at 275 °C) indicating that it is an oxide catalyst. In contrast PrO<sub>1.833</sub> functions for dehydration and dehydrogenation. (8) The decomposition pathway and the composition, structure, surface texture and catalytic activity of the final products are mainly controlled by the atmosphere during the decomposition of PrOx.

## References

- 1 Y. Wilbert, A. Duquesnoy and F. Marion, *C.R. Acad. Sci. Paris*, 1966, **263**, 1539.
- 2 B. G. Hyde, D. J. M. Bevan and L. Eyring, *Philos. Trans. R. Soc. London*, 1966, **259**, 583.
- 3 L. Eyring and N. C. Baenziger, *J. Appl. Phys. Suppl.*, 1962, **33**, 428.
- 4 J. M. Hong, A. F. Clifford and P. A. Faeth, *Inorg. Chem.*, 1962, **2**, 719.
- 5 S. S. Moosath, J. Abraham and T. V. Swaminathan, *Z. Anorg. Chem.*, 1963, **324**, 90.
- 6 K. Muraishi, H. Yokobayashi and K. Nagase, *Thermochim. Acta*, 1991, **182**, 209.
- 7 L. M. Dassuncao, I. Giolito and M. Ionashiro, *Thermochim. Acta*, 1989, **137**, 319.
- 8 G. A. M. Hussein, *J. Anal. Appl. Pyrolysis*, 1994, **29**, 89.
- 9 S. A. Mansour, G. A. M. Hussein and M. I. Zaki, *Thermochim. Acta*, 1989, **150**, 153.
- 10 G. A. M. Hussein, *J. Powder Tech.*, 1994, **80**, 265.
- 11 D. L. Trimm and A. Stanislaus, *Appl. Catal.*, 1986, **21**, 215.
- 12 G. A. M. Hussein and H. M. Ismail, *J. Colloid Surf.*, 1995, in the press.
- 13 K. Tanabe, K. Mismo, Y. Ono and H. Hattori, *New Solid Acids and Bases*, Elsevier, NY, 1989, pp. 41–47.
- 14 G. C. Bond and E. F. Thair, *Appl. Catal.*, 1991, **71**, 1.
- 15 H. Arakawa, *Technol. Jpn.*, 1988, **21**, 32.
- 16 G. A. M. Hussein, N. Sheppard, M. I. Zaki and R. B. Fahim, *J. Chem. Soc., Faraday Trans. 1*, 1989, **85**, 1723.
- 17 K. S. Kim and M. A. Barteau, *J. Mol. Catal.*, 1990, **63**, 103.
- 18 G. A. M. Hussein and H. M. Ismail, *J. Bull. Chem. Soc. Jpn.*, 1994, **67**, 2634.
- 19 J. B. Peri and B. H. Hannan, *J. Phys. Chem.*, 1960, **64**, 1526.
- 20 B. C. Lippens, B. G. Linsen and J. H. de Boer, *J. Catal.*, 1964, **3**, 32.
- 21 J. A. Goldsmith and S. D. Ross, *Spectrochim. Acta, Part A*, 1967, **23**, 1909.
- 22 S. J. Gregg and K. S. W. Sing, *Adsorption, Surface Area and Porosity*, Academic Press, London, 2nd edn., 1982.
- 23 K. S. W. Sing, *Pure Appl. Chem.*, 1982, **54**, 220.
- 24 G. A. M. Hussein, *Thermochim. Acta*, 1991, **180**, 187.
- 25 A. V. Kiselev and A. V. Uvarov, *Surf. Sci.*, 1967, **6**, 399.
- 26 M. I. Zaki and N. Sheppard, *J. Catal.*, 1983, **80**, 114.
- 27 C. Lahoue, A. Aboulayt, F. Mauge, J. Bachelier and J. C. Lavalley, *J. Mol. Catal.*, 1993, **84**, 284.

Paper 4/05964F; Received 29th September, 1994